Correlations of crystallographic defects and anisotropy with magnetotransport properties in Fe_{x}TaS_{2} single crystals (0.23≤x≤0.35)

Chih-Wei Chen, Shalinee Chikara, Vivien S. Zapf, and E. Morosan

Phys. Rev. B **94**, 054406 — Published 2 August 2016

DOI: 10.1103/PhysRevB.94.054406

Correlations of crystallographic defects and anisotropy with the magneto-transport properties in Fe_xTaS_2 single crystals ($0.23 \leq x \leq 0.35$)

Chih-Wei Chen,[1] Shalinee Chikara,[2] Vivien S. Zapf,[2] and E. Morosan[1]
[1] *Department of Physics and Astronomy, Rice University, Houston, TX 77005 USA*
[2] *National High Magnetic Field Laboratory, Los Alamos National Laboratory, Los Alamos, NM 87545 USA*
(Dated: July 12, 2016)

Very large magnetoresistance discovered in single crystals of the ferromagnetic Fe-intercalated transition metal dichalcogenide, $Fe_{0.28}TaS_2$ was attributed to the deviation of the Fe concentration from commensurate values ($x = 1/4$ or $1/3$), which caused magnetic moment misalignments. Here we report a study of Fe_xTaS_2 crystals with $0.23 \leq x \leq 0.35$, demonstrating that crystallographic defects lead to spin disorder, which correlates with magneto-transport properties such as switching magnetic field H_S, magnetoresistance MR, and even zero-field resistivity ρ_0 and temperature coefficient A in $\rho(T) = \rho_0 + AT^2$: The ordering temperature T_C and Weiss temperature θ_W are maximized at the superstructure composition $x = 1/4$, while H_s, MR, ρ_0, and A are minimum. Conversely, at a composition intermediate between the superstructure compositions $x = 1/4$ and $1/3$, the corresponding magneto-transport properties reach local maxima.

PACS numbers: 75.30.Gw, 75.47.De, 75.47.-m

I. INTRODUCTION

Magnetoresistance (MR) is the change in resistivity with applied magnetic field. The ordinary magnetoresistance in bulk metals is generally a few percent.[1] In contrast to bulk metals, Baibich et al.[2] discovered giant magnetoresistance (GMR) in two dimensional Fe/Cr magnetic superlattices, where MR can be as large as 60%. Since then, intense interest has arisen due to potential industrial applications, and GMR was observed in more magnetic/non-magnetic/magnetic heterostructures.[3–11] The GMR[2] in these heterostructures was qualitatively explained by a two-current model,[12,13] where spin-up and spin-down electrons had different resistivities due to their opposite alignment with the magnetization of a magnetic layer. This resulted in a spin-up current and spin-down current, which, in turn, generated either a high or a low resistivity state, due to the relative alignment of the magnetization in the different magnetic layers.

The antiparallel magnetization between magnetic layers in magnetic/non-magnetic/magnetic heterostructures was attributed to the RKKY interactions.[16] These antiparallel alignments mediated by the RKKY interaction were supported by the thickness dependence of the interplane coupling strength.[16] The concept of antiparallel alignment was later generalized to the misalignments of spins.[14,15] Although GMR was predominantly observed in two dimensional systems due to the increased interfacial scattering where the misalignment occurred, the same physics could take place in some 3D systems where ferromagnetic clusters were immersed in a non-magnetic matrix.[15,17] The GMR in both 2D and 3D systems indicates that the misalignment of magnetic moments is crucial to produce a large magnetoresistance.[14,15,17]

Meanwhile, materials that have large MR are still rare and in demand. To search for new materials that have large MR, beyond 2D heterostructures, ferromagnetic materials that can easily have misalignments of the magnetic moments are preferred. In the ongoing research, intercalated transition metal dichalcogenides may be ideal candidates because of the potential for tuning their magnetic properties through different types or amounts of intercalants,[18–20] and their inherent potential for large magnetic anisotropy. Fe-intercalated TaS_2 has a ferromagnetic ground state for $x = 0.23$ to 0.4 in Fe_xTaS_2 with the magnetic easy axis along c axis, which is perpendicular to the TaS_2 planes.[18,19] When x is equal to $1/4$ or $1/3$, the intercalated Fe ions form commensurate $2a \times 2a$ or $\sqrt{3}a \times \sqrt{3}a$ superlattices respectively.[18,19]

Recently, large MR was discovered in $Fe_{0.28}TaS_2$,[21] when a minute ($\Delta x = 0.03$) Fe concentration departure from the $Fe_{1/4}TaS_2$ superstructure resulted in an increase of MR close to two orders of magnitude.[22] It was suggested that the large MR in the $Fe_{0.28}TaS_2$ single crystals was due to the magnetic disorder scattering. Here we report magnetization and MR of ferromagnetic Fe_xTaS_2 single crystals with various Fe concentrations. Our results suggest that the MR in Fe_xTaS_2 indeed results from the magnetic disorder scattering, which is due to the misalignment of the magnetic moments. In turn, the misalignment is attributed to crystallographic defects such as vacancies due to the deviation from the commensurate Fe concentrations (1/4 or 1/3), or the antiphase boundaries,[23,24] or both. Surprisingly, even larger magnetoresistance is now unveiled in $x = 0.297$ single crystals: even though the $T = 2$ K magneto-transport properties fall in line with the trend as a function of Fe content x, just a small temperature increase to $T = 2.3$ K results in a remarkable increase in MR to 140%. This observation is consistent with the disorder-enhanced MR scenario, and underlines the complexity of the magneto-transport properties in Fe_xTaS_2, and their correlations with the crystallography. This identifies a plausible pathway to enhanced controllable MR, in magnetic systems just off from crystallographic order, or with otherwise

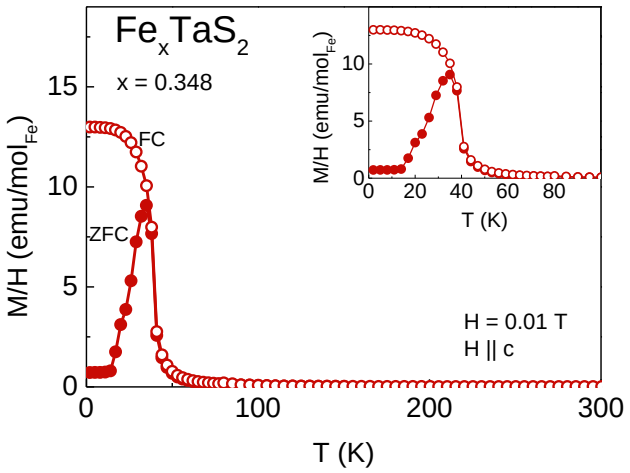

FIG. 1: ZFC (solid circles) and FC (open circles) temperature-dependent magnetic susceptibility M/H of $Fe_{0.348}TaS_2$, with $H = 0.01$ T ($H \parallel c$), with the low temperature range shown in the inset.

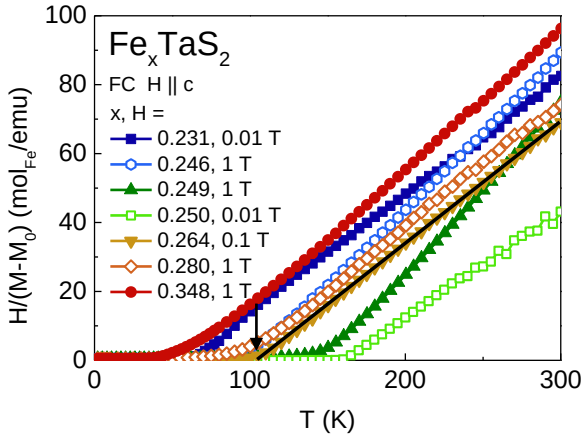

FIG. 2: The inverse magnetic susceptibility H/M (symbols) of Fe_xTaS_2, $x = 0.231, 0.246, 0.249, 0.25$ (from ref.[20]), 0.264, 0.280, and 0.348, together with an example of the Curie-Weiss fit at high temperatures (solid line), with a vertical arrow marking the Weiss temperature θ_W.

enhanced disordered magneti scattering.

II. METHODS

Fe_xTaS_2 single crystals were prepared using iodine vapor transport in a sealed quartz tube, as described elsewhere.[22] The typical size of the resulting single crystals was $2\times2\times0.1$ mm^3. The Fe concentration was determined from Inductively Coupled Plasma Optical Emission Spectroscopy (ICP-OES) measurements conducted by Galbraith Laboratories, Inc.. The determined Fe concentration has an error less than 2% of the reported x values. Temperature- and field-dependent magnetization data were collected in a Quantum Design (QD) Magnetic Property Measurement System (MPMS) and a Vibrating Sample Magnetometer in a 14 T Physical Properties Measurement System (PPMS). Temperature and magnetic field-dependent DC resistivity measurements were also performed in a QD PPMS using standard four-probe methods with the current $i \parallel$ab.

III. RESULTS

The magnetic susceptibility M/H for Fe_xTaS_2 single crystals with x between 0.23 and 0.35 has been measured anisotropically, with an applied field H = 0.01 T. Within this concentration region, Fe_xTaS_2 had been reported to order ferromagnetically. This is indeed confirmed by the temperature-dependent magnetic susceptibility, as exemplified by the zero field-cooled (ZFC) (full symbols) and field-cooled (FC) (open symbols) data shown in Fig. 1 for x = 0.348. At high temperatures, Curie-Weiss behavior is signaled by the linear inverse susceptibility H/(M - M$_0$) (Fig. 2), after a temperature independent magnetization contribution $\chi_0 = M_0/H$ has been accounted for. The effective moment μ_{eff} values, which are derived from the linear fits of the inverse susceptibility at high temperatures, are between 3.95 and 5.88 μ_B/Fe. The magnetic susceptibility significantly increases upon cooling through the ferromagnetic order at T_C (Fig. 1). The T_C values are determined from both the magnetization derivative dM/dT (open symbols, left axis, inset of Fig. 3a), and from the resistivity data shown below. All T_C, μ_{eff}, and χ_0 for all Fe_xTaS_2 compounds in this study are listed in Table 1.

The $H = 0$ temperature-dependent resistivity data $\rho(T)/\rho(300\text{K})$ are shown in Fig. 3a, with the inset illustrating how T_C is determined, from the minimum or maximum in the derivatives of the magnetic susceptibility (left axis) and resistivity data (right axis). The weakly linear decrease in $\rho(T)/\rho(300K)$ above T_C is indicative of poor metal behavior, while a drop below T_C is consistent with the loss of spin disorder scattering at the FM ordering.[22] Furthermore, power law behavior $\rho(T) = \rho_0 + AT^2$ is evident for $x > 0.231$ at low temperatures. Fig. 3b-d exemplifies the linear ρ vs. T^2 behavior for compositions around the commensurate $x = 0.25$ value, while pointing to a minimum in the quadratic temperature coefficient A exactly at x = 0.25. Not surprisingly, the residual resistivity value ρ_0 is also minimized for the ordered superstructure, and the ρ_0 and A values across the series are listed in Table 1.

The temperature-dependent data paint a picture of non-monotonous dependence on x of the magneto-transport properties in Fe_xTaS_2, with a singularity at the superstructure composition x = 0.25: maximum Weiss θ_W and Curie T$_C$ temperatures, minimum ρ_0 and A in $\rho(T) = \rho_0 + AT^2$. Even more remarkable behavior is unveiled by the field-dependent magnetization and resistivity measurements with field applied along the mag-

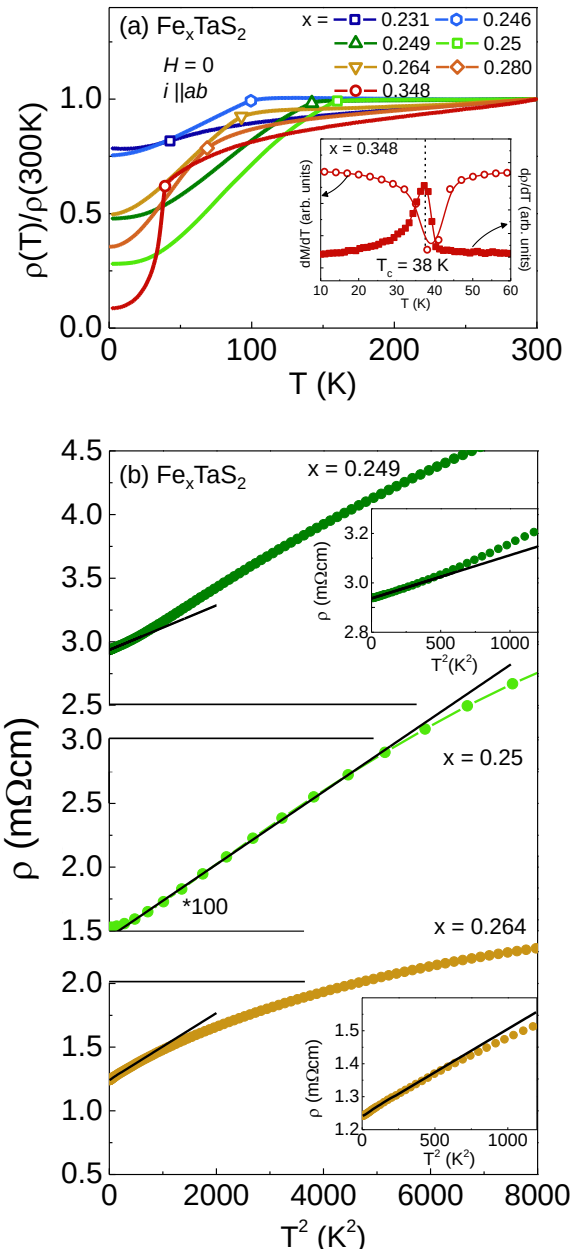

FIG. 3: (a) Temperature-dependent resistivity of Fe_xTaS_2 single crystals (x = 0.231, 0.246, 0.249, 0.264, 0.280, and 0.348) with $H = 0$ and $i \parallel ab$. The symbols mark the Curie temperature T_C as determined from dM/dT and $d\rho/dT$ as illustrated in the inset for $x = 0.348$ (open symbols, left axis and full symbols, right axis, respectively). Data for $x = 0.28$ is from ref.[20]. (b) $\rho(T)$ *vs.* T^2 for x = 0.249, 0.250, and 0.264, with solid lines representing fits to $\rho(T) = \rho_0 + AT^2$. The insets show the low temperature range for clarity.

netic easy axis ($H \parallel c$). When $x > 0.231$, the magnetization isotherms $M(H)$ (Fig. 4) reveal sharp magnetization switching, similar to that reported for the $Fe_{0.25}TaS_2$[22] and $Fe_{0.28}TaS_2$.[21] For $x = 0.231$ (Fig. 4a), no sharp switching behavior was observed down to 2 K, and $M(H)$ shows a typical hysteresis loop with a coercive field $H_c \leq 5.5$T for $T \geq 2$ K. The H_s or H_c values are listed in Table I. Even though the M(H) isotherms do become more square for compositions 0.231 < x < 0.25 (Fig. 4b,c), their magnetization reaches only $M \simeq 3\mu_B$/Fe at the maximum field for our measurements, smaller than the saturated moment $M[9T] \simeq 4\ \mu_B$/Fe for all other compositions. The less than μ_{sat} magnetization for the $x < 0.25$ is likely a result of larger field scale for saturation in this composition, consistent with the finite $M(H)$ slope at teh maximum applied field.

A more complete picture of the magnetic properties of Fe_xTaS_2 can be drawn in conjunction with magnetoresistance MR measurements, with MR given by:

$$\mathrm{MR} = \frac{\Delta\rho}{\rho_0} = \frac{\rho(H) - \rho(0)}{\rho(0)}.$$

The MR measurements, with magnetic field H applied along the c axis, were performed at selected temperatures for all compounds (Fig. 5 and Fig. 6). Below T_C, as the magnetic field H increases from 0 to 9 T, MR of all single crystals with $x > 0.231$ increases to a maximum value at H_S, and then drops in a very narrow field interval ΔH, followed by a nearly linear decrease up to the maximum measured field $H = 9$ T. When the magnetic field direction is reversed, the same change in MR is observed, resulting in a bow-tie shape of MR. For $x = 0.231$, the bow-tie MR is more rounded than in the larger compositions. This is qualitatively consistent with rounded $M(H)$ loops. The MR of $x = 0.264$ crystal at 2 K appears to have a smaller value than the one at 4 K. This is due to H_s of this crystal being close or higher than the maximum applied field H = 9 T, and therefore no switching is observed at $T = 2K$ within our field range. An even more remarkable and non-monotonous change of MR with temperature occurs for the two compositions (x = 0.297 and 0.308) closest to the $x = 0.33$ superstructure composition (Fig. 6). A minute change in temperature from $T = 2$ K to 2.3 K results in tripling the MR for x = 0.297 (Fig. 6a), for a maximum of nearly 140% at T = 2.3 K, with a similar increase, albeit smaller, for x = 0.308 (Fig. 6b).

The H_s values determined from the MR data are consistent with those from $M(H)$ measurements, while the absolute MR values vary greatly with x, even when $M(H)$ data show little composition dependence. For $0.246 \leq x \leq 0.348$, the $M(H)$ shows nearly flat plateaus between -H_s and H_s, with small departures from $\mu_{sat} \simeq 4\mu_B$/Fe only close to the switching field (Fig. 4b-f). However, the MR varies over nearly two orders of magnitude within this composition range, with a minimum MR[2K] $\simeq$ 1% for $x = 0.25$ (ref. [20]) and a maximum MR[2.3K] $\simeq$ 140% for $x = 0.297$ (Fig. 6). While the minimum at the $x = 0.25$ superstructure composition can be readily understood within the picture of an ordered Fe sublattice, the maximum at $x = 0.297$ is less readily apparent, but a likely explanation is offered in the following Discussion section.

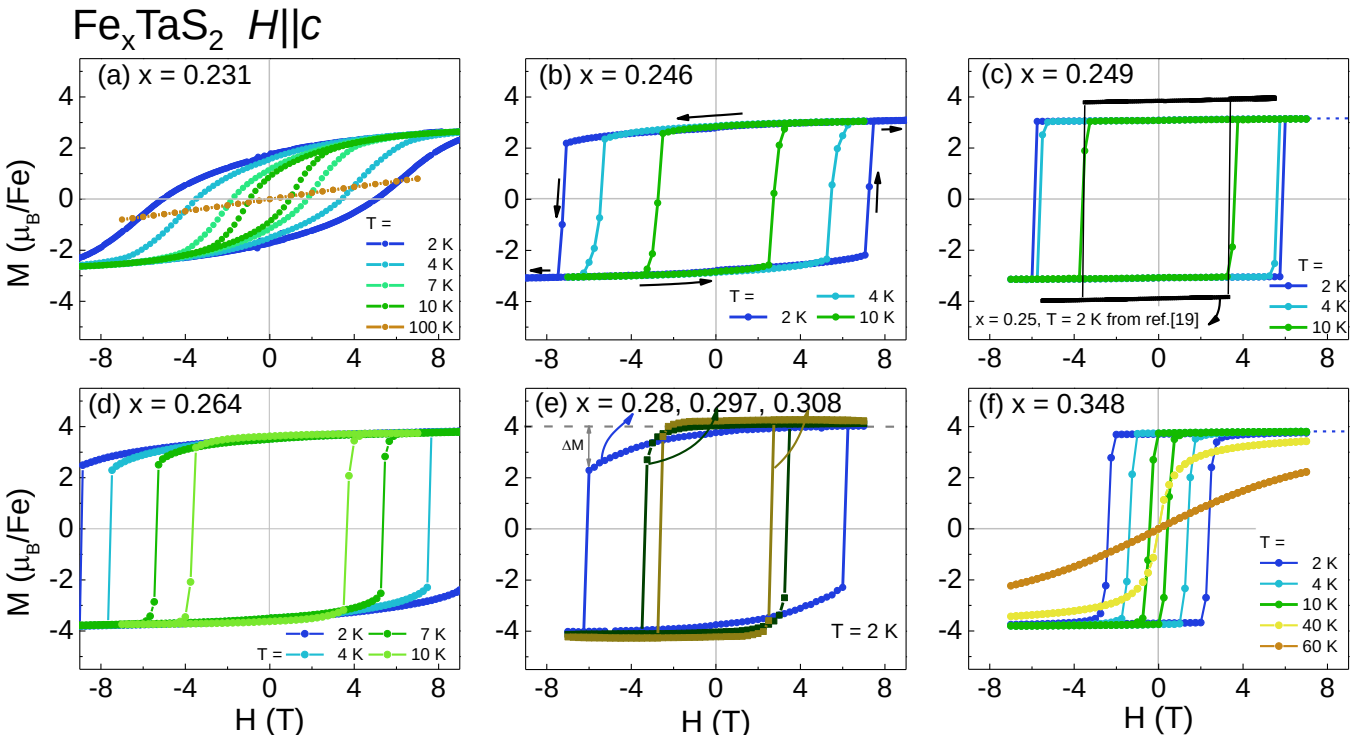

FIG. 4: $H \parallel c$ magnetization isotherms $M(H)$ for Fe_xTaS_2 for x = (a) 0.231 , (b) 0.246, (c) 0.249, (d) 0.264, (e) 0.280, 0.297, 0.308, and (f) 0.348. The data for $x = 0.25$ and $x = 0.280$ are reproduced from references [20] and [19], respectively. Arrows in (b) indicate the field sweep direction.

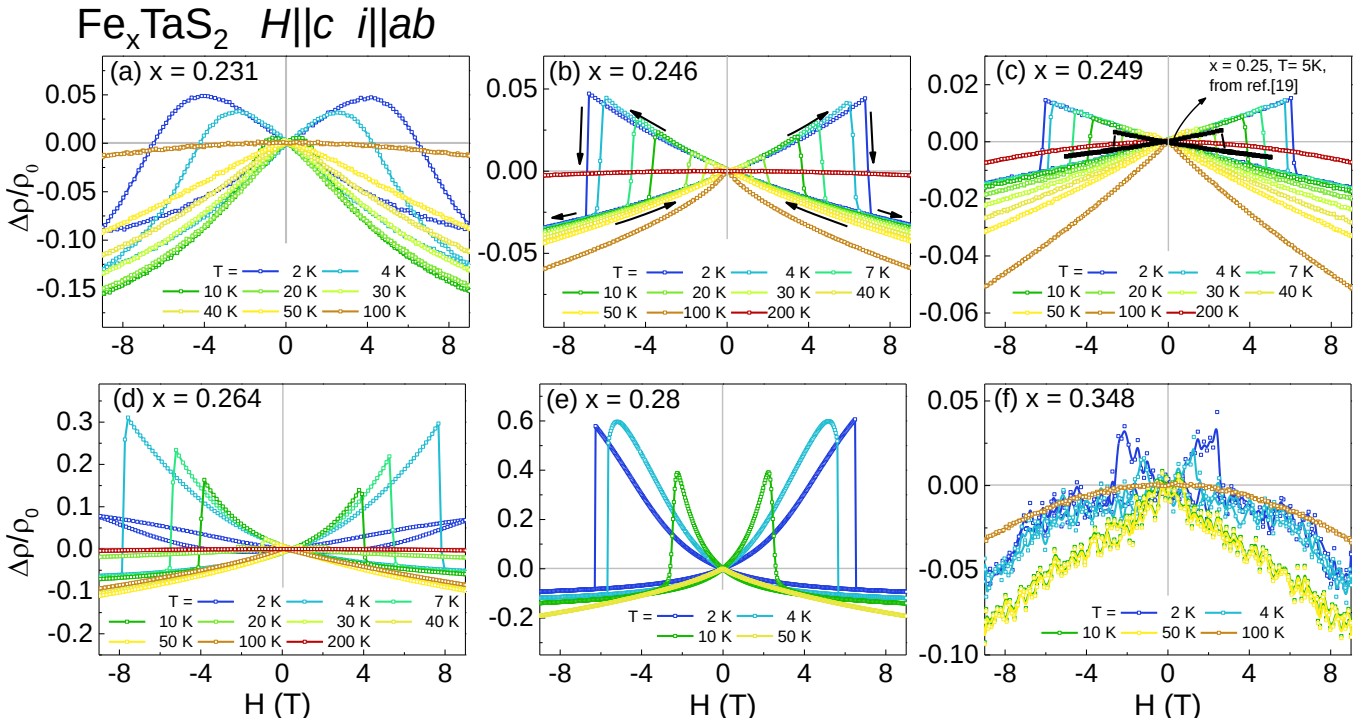

FIG. 5: Magnetoresistance of Fe_xTaS_2 x = (a) 0.231 , (b) 0.246, (c) 0.249, (d) 0.264, (e) 0.280, and (f) 0.348. The data for $x = 0.25$ and $x = 0.280$ are reproduced from references [20] and [19], respectively. Arrows in (b) indicate the field sweep direction.

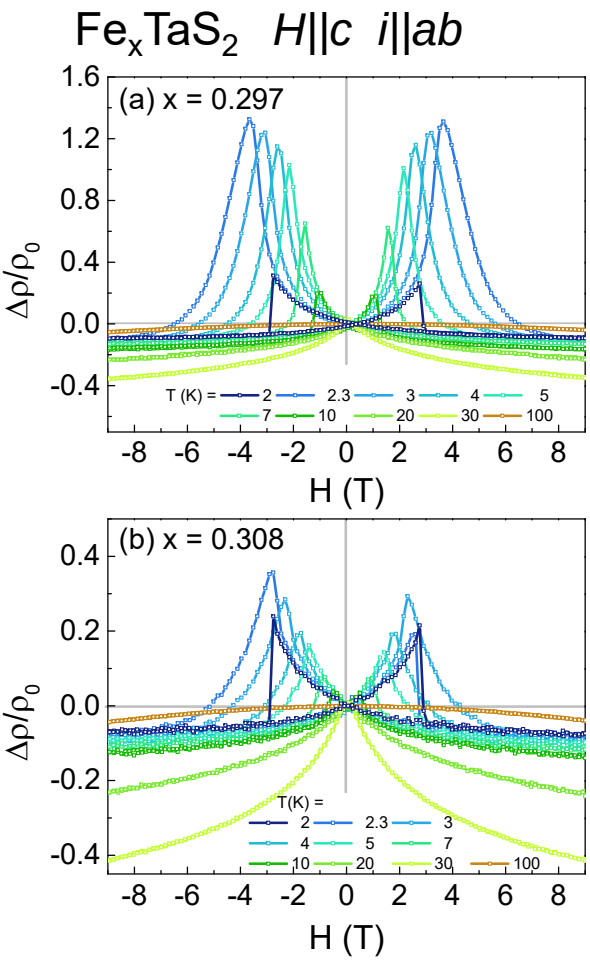

FIG. 6: Magnetoresistance of Fe_xTaS_2 x = (a) 0.297, (b) 0.308.

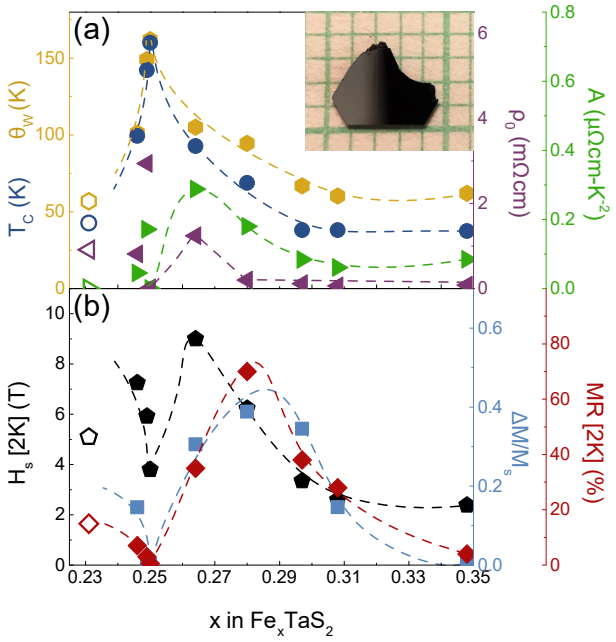

FIG. 7: (a) T_C (hexagons, left axis), θ_W (circles, left axis), ρ_0 (left triangle, right axis), and A (right triangle, right axis) in $\rho(T) = \rho_0 + AT^2$ as a function of x in Fe_xTaS_2. (b) H_s (pentagon, left axis), $\Delta M/M_s$ (squares, right axis), and MR (diamond, right axis). An example of a Fe_xTaS_2 single crystal is shown in the inset in (a). Open symbols indicate the absence of sharp switching behavior in the $x = 0.231$ compound.

Qualitatively, when $T < T_C$, crystals that have sharp switching behavior share similar field-dependence in MR measurements, with bow-tie shape and non-monotonous change in MR values with x. When $T > T_C$, the bow-tie shape disappears, and MR of all samples decreases monotonically with increasing magnetic field (Fig.5).

IV. DISCUSSIONS

A summary of the magneto-transport properties of Fe_xTaS_2 is shown in Fig. 7. The striking non-monotonous change in the Curie temperature T_C (hexagons) and the Weiss temperature θ_W (circles) (top panel) results in a maximum at the superstructure composition $x = 0.25$. All other properties of Fe_xTaS_2, such as the residual resistivity ρ_0 (left triangles) and the resistivity coefficient A (right triangles) in the $H = 0$ $\rho(T) = \rho_0 + AT^2$ (Fig. 7a), the switching field H_s (pentagons), and MR at low temperatures (diamonds) (Fig. 7b), all display minima at the same superstructure composition, while their respective values are maximized at intermediate compositions between the two known superstructures at x = 1/4 and 1/3. In particular, very large MR ($\sim$ 140%) is observed in $Fe_{0.297}TaS_2$ (Fig. 6a). Very large MR in $Fe_{0.28}TaS_2$ was previously attributed to magnetic disorder scattering,[21,22] described below, but a scenario that accounts for why this large MR occurs at these particular compositions can only be offered based on the current comprehensive composition study.

Because Fe_xTaS_2 has the magnetic easy axis along the c axis, together with significant anisotropic magnetization and sharp switching behavior,[21,22] an Ising model can be used to describe its magnetic properties. When all magnetic moments are parallel to the c axis and the external magnetic field, there is little or no magnetic disorder scattering. Once an opposite magnetic field is applied, some magnetic moments are flipped and form antiparallel pairs with neighboring magnetic moments. The pairs function as carrier scatterers and produce increased resistivity. When the magnetic field is larger than a critical value H_s, all magnetic moments are flipped and aligned with the external field, and consequently the MR decreases with the lack of scattering off of antiparallel spin pairs.

Because the resistivity depends on the fraction of these antiparallel pairs, the formation of additional pairs before reaching H_s results in a relatively larger resistivity. The amount of antiparallel pairs can be estimated from the

magnetization measurements, because the formation of antiparallel pairs reduces the magnetic moment from its saturation value μ_{sat}. Therefore, the relative decrease of the magnetic moment:

$$\frac{\Delta M}{M_s} = \frac{M[9T] - M[-H_s + 0]}{M[9T]}$$

before the sharp switching (illustrated in Fig. 4e) can be used as a measure of the number of antiparallel spin pairs. The $\Delta M/M_s$ dependence on x is captured in Fig. 7b (squares). The H_s and MR values correlate with $\Delta M/M_s$, all being minimum at x = 0.25. More remarkable is that the maximum in all these values appears at some intermediate composition between the two superstructures at x = 1/4 and 1/3.

The $\Delta M/M_s$ correlation with MR was also observed in 2D and 3D ferromagnetic systems, such as $Ni_{81}Fe_{19}$ layers separated by non-magnetic Cu layer,[14] and ferromagnetically inhomogeneous Cu-Co alloys,[15,17] and was attributed to the misalignment of the spins.[14,15,17] There are also substantive differences between Fe_xTaS_2 and other magnetic systems mentioned previously,[14,15,17] most significantly that the magnetic moments in Fe_xTaS_2 flip along the c axis at H_s instead of tilting off the c axis.[21,22]

The large MR at intermediate ferromagnetic compositions in Fe_xTaS_2 and the non-monotonous change in MR with x prompt the need for understanding the magneto-transport mechanism in these systems. By contrasting the small (< 1%) MR in the commensurate (ordered) x = 0.25 compound[22] with the very large MR (140%) in x = 0.297 single crystals, the disorder in the magnetic Fe sublattice is readily apparent.

For $x = 1/4$ and $x = 1/3$, Fe ions form a $2a \times 2a$ and $\sqrt{3}$a $\times$ $\sqrt{3}$a superstructure respectively, and all magnetic moments have the same coupling strength with their neighbors. However, when the Fe concentration deviates from these specific superstructure values, some vacancies are created and the magnetic moments near these vacancies have smaller coupling strength with their neighbors. As a consequence, the magnetic moments near the vacancies will be more easily flipped when the opposite magnetic field is applied, and antiparallel pairs are created. This argument is supported by the observation that $\Delta M/M_s$ has a minimum value when x is close to the commensurate concentration $x = 0.25$ and increases when x deviates from this superstructure composition (Fig. 7a). It also explains the maximum MR of $x = 0.297$ crystals, a composition very close to the average of 0.25 and 0.33, where this disorder is likely maximized.

The domain wall is a place where antiparallel spin pairs can occur. This contribution to the MR was estimated to be negligible due to the observation of large MR in a relatively small number of domain walls in exfoliated $Fe_{0.28}$TaS2 crystals.[21] Meanwhile, a magneto-optic study[26] on $Fe_{0.25}TaS_2$ showed that the magnetic domains in this crystal were of micrometer size, which was considered to be too large to significantly contribute to MR. Although the domain wall had a negligible contribution to MR in Fe_xTaS_2 crystals, it is still worth pointing out that further magneto-optic studies on these Fe_xTaS_2 crystals can reveal more details on the correlations between iron concentration and domain wall evolution.

Another source of the antiparallel spin pairs is the existence of phase boundaries between two commensurate superlattices ($2a \times 2a$ or $\sqrt{3}a \times \sqrt{3}a$), and the antiphase boundaries, where the atomic configuration is different from a perfect arrangement within each commensurate superlattice. Both types of boundaries can coexist for the same average Fe concentration within one crystal.[23,24] It was also suggested that the boundaries could cause pinning effects that affected the magnetic properties in Fe_xTaS_2 compounds, such as H_s or H_c.[23,24] When a Fe_xTaS_2 crystal has more boundaries, which means smaller domain size, the pinning effect is stronger. This yields a larger H_s value even though the Fe concentration is fixed. This explains the different H_s values reported for the same Fe concentrations.[23,25] The fact that, in the current study, H_s and other magneto-transport properties (ρ_0, A, $\Delta M/M_s$, and MR) are correlated, suggests that the single crystals have homogeneous compositions, and therefore little or no phase boundaries.

Of note is the qualitative change in the shape of the MR curves at $T > 2$ K for the $x = 0.297$ and 0.308 samples: while at $T = 2$ K, the MR drop at H_s is abrupt for all compositions $x > 0.231$, this remains sharp for compositions away from $x = 1/3$ (Fig. 5), and becomes broader with just a small temperature increase ($T = 2.3$ K) for $x = 0.297$ and 0.308 (Fig. 6). Several scenarios can account for this change and the largest MR up to 140% in the studied compositions.

The first possibility is that the MR for the exact superstructure compositions $x =$ and 1/3 is minimized with the lack of disorder. Departures from the ordered superstructures at intermediate compositions between $x = 1/4$ and 1/3 result in an increase in the magneto-transport properties, including MR, $\Delta M/M_s$ and H_s. This scenario does not account for the peak in the Curie temperature T_C at $x = 1/4$, but a monotonous decrease of T_C with x even through $x = 1/3$. However, this latter superstructure composition has remained ellusive throughout this study. It is also possible that the exact $x = 1/3$ composition may have been inaccurately attributed to systems with x very close to this superstructure composition, given that the electron difraction images (based on which the superstructure was determined) could not detect deffects or small departures from the exact x = 1/3 composition.

A second scenario could come from a change of anisotropy for $x \gtrsim 0.3$. If the Ising model no longer holds, and the moments could cant away from the c axis, this too could lead to enhanced disorder scattering and large MR, while the MR drop at H_s would become broader. This would then allow for a weakening of the ferromagnetic coupling, with a possible antiferromagnetic com-

ponent within the ab plane. While a more remote possibility, this may explain the continuous decrease in T_C with increasing x. Angular-dependent magnetization and magnetoresistance measurements may help validate one of these scenarios, and in turn, provide a potential path to controllably large MR values.

Although most of our compounds show sharp switching behavior in both $M(H)$ (Fig. 4) and $\rho(H)$ (Fig. 5), this behavior is absent in the $x = 0.231$ crystals while the magnetization and field-dependent resistivity are the same as those reported in the ferromagnetically inhomogeneous alloy $Co_{16}Cu_{84}$.[17] This implies that the magnetic moment in $Fe_{0.231}TaS_2$ may be more Heisenberg-like instead of a simple Ising.

V. CONCLUSIONS

In this study, we report the magneto-transport properties of ferromagnetic Fe_xTaS_2 compounds with $x = 0.23$ to 0.35 (Fig. 7). Our results suggest that strong axial anisotropy, combined with crystallographic defects (including vacancies and possible antiphase boundaries), induces the misalignment of magnetic moments. In turn, this misalignment is the cause of large MR in Fe_xTaS_2 single crystals up to 140% at compositions intermediate between the two superstructures at $x = 1/4$ and $1/3$. We provide an explanation for the large MR in Fe_xTaS_2, which may be further applied to other highly anisotropic ferromagnets in the search for new materials with large MR.

VI. ACKNOWLEDGEMENTS

This work was support by the Gordon and Betty Moore Foundation EPiQS Initiative through the grant GBMF4417. Work at the NHMFL Pulsed-Field Facility is funded by the US National Science Foundation through Cooperative Grant No. DMR-1157490, the State of Florida, and the US Department of Energy. CWC and EM thank Dr. D. Natelson for very useful discussions.

[1] T. McGuire and R. Potter, Magnetics, IEEE Transactions on **11**, 1018 (1975).
[2] M. N. Baibich, J. M. Broto, A. Fert, F. Nguyen Van Dau, F. Petroff, P. Etienne, G. Creuzet, A. Friederich, and J. Chazelas, Phys. Rev. Lett. **61**, 2472 (1988).
[3] S. S. P. Parkin, N. More, and K. P. Roche, Phys. Rev. Lett. **64**, 2304 (1990).
[4] S. S. P. Parkin, Z. G. Li, and D. J. Smith, Appl. Phys. Lett. **58**, 2710 (1991).
[5] F. Petroff, A. Barthélemy, D. H. Mosca, D. K. Lottis, A. Fert, P. A. Schroeder, W. P. Pratt, R. Loloee, and S. Lequien, Phys. Rev. B **44**, 5355 (1991).
[6] S. S. P. Parkin, Appl. Phys. Lett. **60**, 512 (1992).
[7] K. Inomata and Y. Saito, Appl. Phys. Lett. **61**, 726 (1992).
[8] Y. Saito, S. Hashimoto, and K. Inomata, Appl. Phys. Lett. **60**, 2436 (1992).
[9] K. Shintaku, Y. Daitoh, and T. Shinjo, Phys. Rev. B **47**, 14584 (1993).
[10] Chengtao Yu, Shuxiang Li, Wuyan Lai, Minglang Yan, Yizhong Wang, and Zhenxi Wang, Phys. Rev. B **52**, 1123 (1995).
[11] M. L. Yan, W. Y. Lai, Y. Z. Wang, S. X. Li, and C. T. Yu, J. Appl. Phys. **77**, 1816 (1995).
[12] A. Fert and I. A. Campbell, J. Phys. F **6**, 849 (1976).
[13] I. A. Campbell and A. Fert, edited by E. P. Wohlfarth *Ferromagnetic Materials*, Vol. 3, p.747, North-Holland Publishing Company, (1982).
[14] B. Dieny, V. S. Speriosu, S. S. P. Parkin, B. A. Gurney, D. R. Wilhoit, and D. Mauri, Phys. Rev. B **43**, 1297 (1991).
[15] A. E. Berkowitz, J. R. Mitchell, M. J. Carey, A. P. Young, S. Zhang, F. E. Spada, F. T. Parker, A. Hutten, and G. Thomas, Phys. Rev. Lett. **68**, 3745 (1992).
[16] J. Unguris, R. J. Celotta, and D. T. Pierce, Phys. Rev. Lett. **67**, 140 (1991).
[17] J. Q. Xiao, J. S. Jiang, and C. L. Chien, Phys. Rev. Lett. **68**, 3749 (1992).
[18] S. S. Parkin and R. H. Friend, Philos. Mag. B **41**, 65 (1980).
[19] S. S. Parkin and R. H. Friend, Philos. Mag. B **41**, 95 (1980).
[20] H. Narita, H. Ikuta, H. Hinode, T. Uchida, T. Ohtani, and M. Wakihara J. Solid State Chem. **108**, 148 (1994).
[21] Will J. Hardy, Chih-Wei Chen, A. Marcinkova, Heng Ji, Jairo Sinova, D. Natelson,and E. Morosan, Phys. Rev. B **91**, 054426 (2015).
[22] E. Morosan, H. W. Zandbergen, Lu Li, Minhyea Lee, J. G. Checkelsky, M. Heinrich, T. Siegrist, N. P. Ong, and R. J. Cava, Phys. Rev. B **75**, 104401 (2007).
[23] Y. J. Choi, S. B. Kim, T. Asada, S. Park, Weida Wu, Y. Horibe, and S-W. Cheong EPL (Europhysics Letters) **86**, 37012 (2009).
[24] Yoichi Horibe, Junjie Yang, Yong-Heum Cho, Xuan Luo, Sung Baek Kim, Yoon Seok Oh, Fei-Ting Huang, Toshihiro Asada, Makoto Tanimura, Dalyoung Jeong, and Sang-Wook Cheong, J. Am. Chem. Soc. **136**, 8368 (2014),
[25] M. Eibschütz, S. Mahajan, F. J. DiSalvo, G. W. Hull, and J. V. Waszczak, J. Appl. Phys. **52**, 2098 (1981).
[26] M. D. Vannette, S. Yeninas, E. Morosan, R. J. Cava, and R. Prozorov, Phys. Rev. B **80**, 024421 (2009).

TABLE I: Summary of magnetic and electrical transport properties of Fe_xTaS_2 crystals.

x	0.231	0.246	0.249	0.250[a]	0.264	0.280[b]	0.297	0.308	0.348
T_C (K)	42.7	80.4	137.6	160	89.9	68.8	38	38	38
θ_W (K)	56.8	101.3	149.1	162	105.1	64.6	66.9	60.3	62.0
χ_0 (emu/mol$_{Fe}$)	0.0025	0.0005	0.0005	-0.0005	-0.0002	0.008	0	0	0.002
μ_{eff} (μ_B)	5.88	4.24	3.95	5.03	4.74	4.67	4.85	4.88	4.46
$\mu_{sat} = M$[2K, 9T] (μ_B)	2.59	3.1	3.15	4	3.82	4	4.12	4.21	3.76
H_s[2K] (T)	5.1[c]	7.25	5.92	3.9	9	6.2	3.35	2.59	2.38
$\Delta M/M_s$[2K]	–	0.146	0.099	0.003	0.3056	0.388	0.345	0.144	0.005
ρ[300K] (mΩcm)	1.17	1.08	6.14	0.05	2.50	0.76	0.54	0.54	0.92
ρ_0 (mΩcm)	0.915	0.816	2.940	0.0175	1.242	0.200	0.115	0.065	0.0804
A ($\mu\Omega$cm-K^2)[e]	–	0.0452	0.171	0.0028	0.288	0.18	0.084	0.061	0.0848
MR[2K] (%)	15	8	3	0.5	35[d]	60	140[f]	35[f]	4

a: From reference [20]. b: From reference [19]. c: Coercive field H_c. d: MR at $T = 4$ K.
e: A in $\rho(T) = \rho_0 + AT^2$. f: MR at $T = 2.3$ K.